Spontaneous brightening of dark excitons in GaAs/AlGaAs quantum dots near a cleaved facet

Y. H. Huo,[1,2,3,*] V. Křápek,[4,†] O. G. Schmidt,[5] and A. Rastelli[1]

[1]*Institute of Semiconductor and Solid State Physics, Johannes Kepler University Linz, Linz Institute of Technology, Altenbergerstrasse 69, A-4040 Linz, Austria*

[2]*Hefei National Laboratory for Physical Sciences at Microscale, University of Science and Technology of China, Hefei, Anhui 230026, China*

[3]*CAS-Alibaba Quantum Computing Laboratory, USTC Shanghai branch, Shanghai 201315, China*

[4]*Central European Institute of Technology, Brno University of Technology, Purkyňova 123, 61200 Brno, Czech Republic*

[5]*Institute for Integrative Nanosciences, IFW Dresden, Helmholtzstrasse 20, D-01069 Dresden, Germany*

(Received 18 October 2016; revised manuscript received 13 March 2017; published 27 April 2017)

Dark excitons (DEs) confined in epitaxial quantum dots (QDs) are interesting because of their long lifetime compared to bright excitons (BEs). For the same reason they are usually difficult to access in optical experiments. Here we report on the observation of vertically polarized light emission from DEs confined in high-quality epitaxial GaAs/AlGaAs QDs located in proximity of a cleaved facet of the QD specimen. Calculations based on the eight-band **k·p** method and configuration interaction allow us to attribute the brightening of the DE to the anisotropic strain present at the sample edge, which breaks the symmetry of the system and enhances valence-band mixing. The mechanism of DE brightening is discussed in detail by inspecting both the Bloch and envelope wave functions of the involved hole states. In addition, by investigating experimentally and theoretically QDs with different sizes, we find that the energy separation between DE and BEs tends to decrease with increasing QD height. Finally, the presence of a cleaved facet is found also to enhance the BE fine structure splitting. This work provides a simple method to optically probe dark excitonic states in QDs and shows that the properties of QDs can be significantly affected by the presence of nearby edges.

DOI: 10.1103/PhysRevB.95.165304

I. INTRODUCTION

The simplest low-temperature excitation in a quantum dot (QD) is a neutral exciton consisting of an electron in the lowest confined conduction-band state and a hole in the uppermost valence-band state. Most of the semiconductor QDs obtained by epitaxial growth of zincblende semiconductors, such as GaAs, are characterized by an uppermost valence-band state of heavy-hole (HH) character. The confined hole, with a total angular momentum quantum number $J = 3/2$ and projection $J_z = \pm 3/2$ along the growth direction z, interacts with the confined electron, with spin projection quantum number $S_z = \pm 1/2$, through the Coulomb and exchange interaction, leading to four possible excitonic configurations. Two of them, with total angular momentum of ± 1, are dipole allowed and are thus referred to as "bright excitons" (BEs). The corresponding transition electric-dipole moments are parallel to the growth plane [(001) GaAs for the dots considered here]. The remaining two, with total angular momentum of ± 2, are dipole forbidden and are therefore called "dark excitons" (DEs). Because of their negligible oscillator strength, DEs have been largely neglected compared to BEs. However, because of their much longer lifetime, DEs are interesting for spin storage for quantum information processing [1–3].

To access the optically inactive DEs, different methods and conditions have been used. Examples include the electrical [2] or optical [3] injection of a single electron or hole into afore-prepared DE states, spin-flip interaction with a magnetic impurity [4], two-photon pumping [5], mixing of carrier spins by an in-plane magnetic field [6–11], and mixing hole states induced by built-in strain or shape asymmetries [12–14].

In this paper we report on the observation of DE emission in GaAs/AlGaAs QDs, which are obtained by local Al-droplet etching of AlGaAs. In absence of perturbations, the studied dots are practically unstrained and are characterized by a round shape [15–17], leading to weak hole mixing [17] and strongly suppressed DE emission. In order to access the DEs, we investigate the light emission of QDs located in proximity of a cleaved facet of the sample, using polarization-resolved microphotoluminescence (μ-PL) spectroscopy. The cleaved edge reduces the symmetry of the QD environment and leads to a spontaneous brightening of the DE emission. By using the eight-band $\mathbf{k}\cdot\mathbf{p}$ method and the realistic structure as input, we show that the enhanced optical activity of DEs in QDs stems from anisotropic strain induced by the cleaved edge in its neighborhood and consequent HH–light-hole (LH) mixing. By studying QDs with different sizes, we find that DEs are optically accessible only when the QD size is sufficiently large and disappear for the smallest QDs. We also find that the energy splitting between DE and BE tends to decrease when the QD size increases. These observations are consistent with the results of our calculations. On one hand, this work shows that nearby edges can significantly influence the optical properties of QDs, which is important in view of their integration in nanophotonic structures [18]. On the other hand, it provides a simple method to achieve spontaneous brightening of DEs in QDs, opening up the possibility to have similar dots with and without the DE emission in the same sample.

The paper is organized into eight sections. Section II presents experimental and theoretical methods involved in the study and Sec. III presents the photoluminescence data. In Sec. IV we discuss symmetry factors related to the cleaved

*yongheng@ustc.edu.cn

†krapek@monoceros.physics.muni.cz

edge and conclude that it is a weak strain field with in-plane anisotropy in the vicinity of the edge that makes the dark excitons optically accessible. In Sec. V we discuss the components of the hole wave function in presence of mixing. Section VI is dedicated to the effects of QD size and in Sec. VII we discuss the fine structure splitting and its variation in the presence of the cleaved edge. Section VIII concludes the paper.

II. EXPERIMENTAL AND THEORETICAL METHODS

The experiments were performed on three different QD samples grown on 350-μm-thick intrinsic GaAs(001) substrates using molecular beam epitaxy. The QD heterostructure, grown on a 25-nm-thick AlAs layer, consists of a 200-nm-thick $Al_{0.4}Ga_{0.6}As$ layer with a layer of GaAs QDs in its center. The QDs were obtained as described in Refs. [15,16]: first round-shaped nanoholes were produced on an $Al_{0.4}Ga_{0.6}As$ surface by Al droplets; then the nanoholes were filled by depositing 1, 1.5, and 2 nm of GaAs for the three different samples. Because of capillarity effects, the corresponding QD heights are about 4, 6, and 7.5 nm.

To access the DE signal, which is expected to be polarized along the growth direction [13], we performed polarization-resolved μ-PL measurements by collecting the PL signal from an edge of the samples, cleaved along the [110] crystal direction, using the configuration sketched in Fig. 1(b). Linear polarization analysis was performed using a rotatable achromatic half-wave plate and a fixed Glan-Thompson polarizer. In all the measurements, the temperature was kept at about 9 K.

The interpretation of the experimental data is supported by theoretical calculations. Exciton energies and optical selection rules are calculated using the configuration interaction (CI) approach on top of single-particle calculations based on eight-band **k·p** theory applied to QDs with realistic shape and composition.

The eight-band **k·p** theory is a state-of-the-art method for the calculation of single-particle properties of QDs [19]. Based on the original formulation of **k·p** theory for bulk crystals [20], it was adapted for quantum heterostructures [21]. For direct band gap semiconductors such as GaAs, the wave function is expanded into a series of zone-center Bloch waves $u_n(\mathbf{r})$ with the space-dependent expansion coefficients $\chi_n(\mathbf{r})$ denoted as envelope functions:

$$\psi(\mathbf{r}) = \sum_{n=1}^{8} \chi_n(\mathbf{r}) u_n(\mathbf{r}). \quad (1)$$

Here the summation goes over two conduction bands and six valence bands—heavy-hole band, light-hole band, and spin-orbit split-off band (each doubly degenerate due to spin). When relevant, the effects of strain are incorporated via Pikus-Bir Hamiltonian [22] and piezoelectric potential is calculated and added to the total Hamiltonian. We note that this applies only to the cleaved-edge related strain as the built-in strain due to lattice mismatch in our GaAs/AlGaAs QDs is negligibly small. A numerical implementation consists in a finite difference scheme with a grid step of 1 nm and a typical grid size of 78 × 78 × 30 (i.e., 1.8×10^5) voxels.

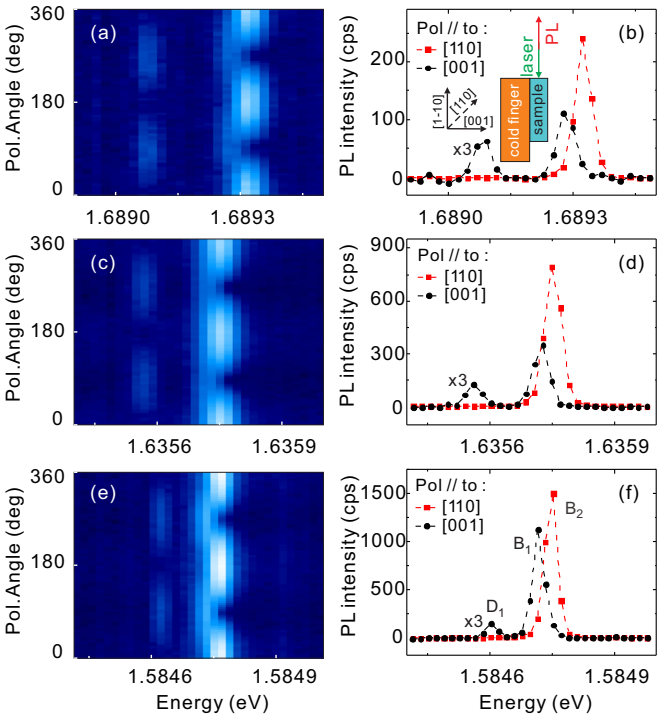

FIG. 1. (a), (c), and (e) Color-coded linear-polarization-resolved spectra collected from a cleaved facet of QD samples with GaAs QDs obtained by filling AlGaAs nanoholes with 1, 1.5, and 2 nm GaAs, respectively. 0° corresponds to the [110] crystal direction, while 90° corresponds to the [001] direction (growth direction). Logarithmic color scale is used for the spectrum intensity. (b), (d), and (f) Spectra extracted from (a), (c), and (e), respectively, at polarization angles of 0° (red squares) and 90° (black circles). D_1 labels the DE component, B_1/B_2 labels the lower/higher components of the BE doublet. The intensity of D_1 and B_1 is magnified by a factor of 3. The insets in (b) show the experimental configuration for the measurements and the sketched crystal directions (the excitation laser and collection path are parallel to the [1–10] crystal direction).

The eigenenergies of the Hamiltonian are found using an optimized Davidson algorithm [23].

The single-particle states were subsequently employed to calculate the exciton structure following the procedure outlined in Refs. [24,25]. Here the exciton wave function is expanded into Slater determinants constructed from the single-particle states. We restricted our basis to the ground electron and hole states and employed optimized evaluation of exchange interaction matrix elements [26].

In the calculations we implemented the nanohole shape measured by AFM to define the lower boundary and a flat plane for the top boundary of the model QD. Such approach was justified in our previous studies [16,27]. The selected height range of the model structures covers the range of the experimentally studied samples.

III. PHOTOLUMINESCENCE SPECTRA FROM A CLEAVED FACET

Figures 1(a), 1(c), and 1(e) show color-coded polarization-resolved spectra obtained from one representative QD contained in each of the three samples discussed above, collected

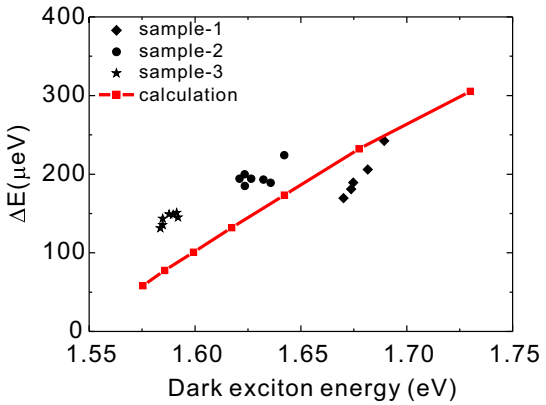

FIG. 2. Experimental and calculated energy separation between DE (D_1) and BE (B_2) as a function of dark exciton energy. The scattered symbols are experimental data. The line plus symbols show the calculated results of QDs with height from 2.6 to 8.6 nm with a step of 1 nm.

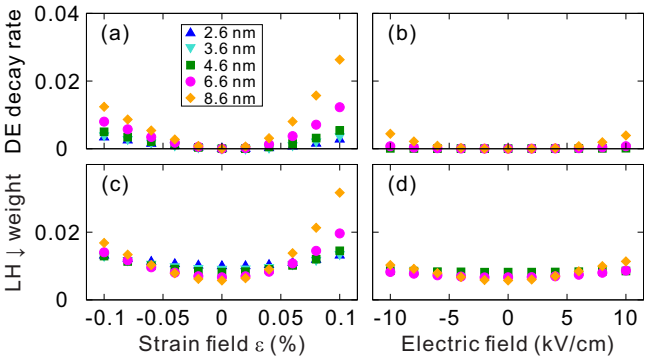

FIG. 3. Relative DE decay rate (divided by the BE decay rate) and $|LH\downarrow\rangle$ weight (in the spin-up hole ground state $\psi_H^{\uparrow}$, which is dominated by $|HH\uparrow\rangle$) as functions of local strain field (a) and (c) and electric field (b) and (d) for several QDs with different sizes. The $|LH\uparrow\rangle$ component is not included because it does not contribute to the optical response (see text). The strain along [1–10] and the electric field along the [1–10] crystal direction are taken as the independent variables.

along the [1–10] direction. Figures 1(b), 1(d), and 1(f) show the corresponding spectra polarized along the [110] and [001] directions. Hereafter we use D_1 to label the DE line, and B_1/B_2 to label the lower/higher energy component of the BE doublet. D_1 appears below B_1/B_2 and is polarized along the [001] direction (i.e., the growth direction, which coincides with the main confinement direction of the QD). Similar observations were reported for CdTe/ZnTe QDs, which are—different from the present case—strongly strained [12]. B_2 appears to be polarized along the [110] direction. B_1 is expected to be polarized along the [1–10] direction. Due to total internal reflection at the interface between the (001) sample surface and air, B_1 can be partially collected along [1–10] as explained in Ref. [17]. Here we point out that in even smaller QDs, obtained by filling the nanoholes with less than 1 nm GaAs, we were not able to detect DE emission.

From Fig. 1 we see that the energy splitting between dark and bright excitonic lines increases with decreasing QD size. The scatter plots in Fig. 2 confirm that the energy splitting ΔE_{DB} between D_1 and B_2 lines measured on different dots in the three different samples tends to increase with increasing exciton energy, i.e., with decreasing QD size.

IV. SYMMETRY-BREAKING FACTORS RELATED TO A CLEAVED FACET

The first question we want to address is: why is the DE visible at all? In the following we will show that the DE brightening stems from the anisotropic strain related to the cleaved edge, which results in enhanced mixing of LHs into dominantly HH-like ground state. Different from the aforementioned works [2–15], our QDs are characterized by very small strain and a regular shape, so that HH-LH mixing in QDs located far away from edges is expected to be small and to have negligible impact on the observability of dark excitons. This statement, which is also supported by atomistic pseudopotential calculations presented in Ref. [17], will be further justified in Sec. V. Because the used materials in our samples are nonmagnetic and the QD has regular shape, the only symmetry-breaking factor is the presence of the cleaved edge. This may introduce (i) an anisotropic strain field with major axis parallel to the [1–10] direction (due to the oxidation of the AlAs layer present below the QD structure, surface reconstruction and oxidation of the cleaved facet, and slight strain relaxation of the Al(Ga)As structure [28]), and/or (ii) a local electric field (from oxidation and surface depletion [29–32]).

To explore the effects of strain and electric field on the visibility of the DE, we used a theoretical model based on eight-band $\mathbf{k}\cdot\mathbf{p}$ theory [19]. The introduced local strain is assumed to have a major component ε along [1–10] (with magnitude up to 0.1%) and a minor component along [001]. The strain along [110] is assumed to be 0 because the layer is fixed to the macroscopic substrate and cannot relax parallel to the cleaved edge [28]. The homogeneous electric field is assumed to be parallel to the [1–10] direction (i.e., perpendicular to the sample edge) with a magnitude up to 10 kV/cm [33].

The results of the calculations are summarized in Fig. 3(a), which shows the values of the DE decay rates relative to the BE decay rates. These values, which are obtained in the dipole approximation [23], roughly correspond to the relative ratio of D_1 and B_2 intensities. The decay rate of the DE is negligibly small if no symmetry-breaking field is present. With increasing strain field the brightness of the DE increases. In addition, the effect is more pronounced for larger QDs, while for smaller QDs the DE decay rate remains small. For the strain $\varepsilon = 0.1\%$, the relative DE decay rates read 0.005, 0.012, and 0.026 for QD heights 4.6, 6.6, and 8.6, respectively. These values have the same order of magnitude as in the experimental data [27]. A direct quantitative comparison is however not possible, since in the experiment we do not know the exact distance of each QD from the cleaved edge, the precise QD shapes, and the values of local strain. By inspecting the wave functions of confined holes as a function of strain we find that the increase of the DE decay rate is accompanied by an enhanced weight of the LHs in the ground hole state (in particular, spin-down LHs

TABLE I. Exciton quadruplet in a QD with the height of 6.6 nm. E is the energy of each exciton component relative to the lowest one. $P_{[110],[1-10],z}$ are the transition probabilities for the emission/absorption with linear polarizations in the respective direction (neglecting a weak elliptical part). The first and second lines correspond to the dark pair, the third and fourth lines correspond to the bright pair.

E (μeV)	$P_{[110]}$	$P_{[1-10]}$	P_z
0	0	0	0
0.9	0	0	0
128.6	0.015	0.863	0
136.1	0.853	0.015	0

for spin-up hole state), as shown in Fig. 3(c). On the contrary, we find that realistic values of electric fields are not sufficient to strengthen the decay rate of DEs to a level comparable to experiments (the weight of the LHs remains negligible), see Figs. 3(b) and 3(d).

The calculated exciton structure in a particular QD (height of 6.6 nm) is detailed in Tables I and II for the case without strain and with strain ($\varepsilon = 0.1\%$), respectively. Without strain, the ground exciton quadruplet is composed of two almost degenerate DEs at low energy and two BEs at higher energy. The DEs are fully optically inactive. The BEs exhibit optical transitions with the linear polarizations close to [110] (high energy) and [1–10] (low energy). The splitting between the BEs (fine structure splitting, FSS) resulting from the slight structural asymmetry of the QD was studied in detail elsewhere [15,16]. The strain produces a brightening of one of the DEs with the polarization along [001], which is more than 50-times weaker than the BE (see Table II). At the same time anisotropic strain also induces an in-plane polarization anisotropy of the bright pair and increases the FSS.

V. MECHANISM OF DARK EXCITON BRIGHTENING

To explain the mechanism of the dark exciton brightening we have to first understand the role of the LH components in the hole state. As stated by Eq. (1), the wave function is represented by an eight-component Luttinger spinor [34]. The zone-center Bloch basis can be conveniently represented in angular momentum representation as $|J, J_z\rangle$ where J and J_z represent quantum numbers of total angular momentum and its z projection. Alternatively, it can be given in Cartesian representation, in which $|S\rangle$ represents the zone-center Bloch wave for conduction band electrons (derived from atomic s orbitals) and $|X\rangle$, $|Y\rangle$, $|Z\rangle$ represent the components of the electron Bloch waves in the valence band (derived from atomic p_x, p_y, p_z orbitals), which transform as the respective coordinates under the crystal point group symmetry operations. The basis states u_n in Eq. (1) read

$$|EL\uparrow\rangle = \left|S, +\frac{1}{2}\right\rangle = |S\uparrow\rangle,$$

$$|HH\uparrow\rangle = \left|\frac{3}{2}, +\frac{3}{2}\right\rangle = \frac{1}{\sqrt{2}}(|X\uparrow\rangle + i|Y\uparrow\rangle),$$

$$|LH\uparrow\rangle = \left|\frac{3}{2}, +\frac{1}{2}\right\rangle = \frac{1}{\sqrt{6}}(|X\downarrow\rangle + i|Y\downarrow\rangle - 2|Z\uparrow\rangle),$$

$$|SO\uparrow\rangle = \left|\frac{1}{2}, +\frac{1}{2}\right\rangle = \frac{1}{\sqrt{3}}(|X\downarrow\rangle + i|Y\downarrow\rangle + |Z\uparrow\rangle),$$

$$|EL\downarrow\rangle = \left|S, -\frac{1}{2}\right\rangle = |S\downarrow\rangle,$$

$$|HH\downarrow\rangle = \left|\frac{3}{2}, -\frac{3}{2}\right\rangle = -\frac{1}{\sqrt{2}}(|X\downarrow\rangle - i|Y\downarrow\rangle),$$

$$|LH\downarrow\rangle = \left|\frac{3}{2}, -\frac{1}{2}\right\rangle = -\frac{1}{\sqrt{6}}(|X\uparrow\rangle - i|Y\uparrow\rangle + 2|Z\downarrow\rangle),$$

$$|SO\downarrow\rangle = \left|\frac{1}{2}, -\frac{1}{2}\right\rangle = \frac{1}{\sqrt{3}}(|X\uparrow\rangle - i|Y\uparrow\rangle - |Z\downarrow\rangle).$$

Here EL, HH, LH, and SO correspond to electrons in the conduction, heavy-hole, light-hole, and spin-orbit split-off bands, respectively. The only nonzero optical matrix element is of the spin-conserving type $\langle S\uparrow|\, p_x|X\uparrow\rangle$ with the polarization direction corresponding to the valence band symmetry (x polarization for $|X\rangle$, etc.). Thus, a heavy-hole corresponding to a missing spin-up electron ($|HH\uparrow\rangle$) can be combined with a spin-up electron $|EL\uparrow\rangle$ to form a bright exciton ($\langle S\uparrow|\, p_x|X\uparrow\rangle$ is nonzero and $\Delta J_z = 1$). In contrast, the same state forms a dark exciton when combined with a spin-down electron $|EL\downarrow\rangle$ ($\langle S\downarrow|p_x|X\uparrow\rangle$ is zero and $\Delta J_z = 2$—such an angular momentum cannot be carried by a single photon).

The ground hole state forms a Kramers doublet and is dominated by a heavy-hole component with a weight of above 90% according to our calculations. [From Eq. (1), the weight of one of the basis bands u_n in the valence-band state ψ_H can be defined as $\langle \chi_n \mid \chi_n \rangle$.] Both states of the Kramers doublet can be combined so their major-spin heavy-hole components are maximized and the minor-spin heavy-hole components are virtually zero. In the following, we refer to these two states as $\psi_H^{\uparrow}$ and $\psi_H^{\downarrow}$ and focus on the $\psi_H^{\uparrow}$ state, which is dominated by the $|HH\uparrow\rangle$ component. As it was explained, a hole in this state forms a BE with the spin-up electron $|EL\uparrow\rangle$ and a DE with the spin-down electron $|EL\downarrow\rangle$. When the light hole corresponding to a missing spin-up electron $|LH\uparrow\rangle$ is mixed to this state, the presence of a $|Z\uparrow\rangle$ component adds an out-of-plane polarized transition to the BE (with $|EL\uparrow\rangle$) and two bright (but weak for moderate HH-LH mixing) in-plane

TABLE II. Exciton quadruplet as in Table I (QD height 6.6 nm) in presence of strain field (tensile strain $\varepsilon = 0.1\%$ along [1–10] with a proper relaxation along [001]).

E (μeV)	$P_{[110]}$	$P_{[1-10]}$	P_z
0	0	0	0.010
2.4	0	0	0
114.5	0.001	0.720	0
149.3	0.975	0	0

polarized transitions to the DE (with $|EL\downarrow\rangle$). The presence of a $|LH\downarrow\rangle$ component in the $\psi_H^{\uparrow}$ may lead instead to a polarization anisotropy of the BE transitions and adds a bright out-of-plane polarized transition to the DE. Our experiment reveals an out-of-plane polarization for DE transitions, which corresponds to the $|LH\downarrow\rangle$ component mixed into the $\psi_H^{\uparrow}$ hole state (and $|LH\uparrow\rangle$ component mixed into $\psi_H^{\downarrow}$ state).

In as-grown QDs without additional strain or electric fields, the LHs are coupled to the dominant HH primarily by the quantum confinement. (Additional effects, such as interface disorder, which are not modified by strain, are discussed in Ref. [35].) In the case considered in Table I (QD height 6.6 nm, no strain) the $|LH\uparrow\rangle$ and $|LH\downarrow\rangle$ weights in the spin-up hole state $\psi_H^{\uparrow}$ are 4.1% and 0.7%, respectively. Despite a small but significant weight of LHs (about 5% in total), mixing does not affect appreciably the optical properties, which are very close to those of a purely HH exciton, i.e., there is no emission with out-of-plane polarization. We note that the dominant LH contribution to the $\psi_H^{\uparrow}$ state is given by $|LH\uparrow\rangle$. According to the form of the Bloch waves (see discussion above), this LH state would induce in-plane polarized emission for the DE and out-of-plane polarized emission for the BEs, in contrast to the experimental data. The reason can be understood by inspecting the envelope functions of the hole wave functions and their overlap with the electron wave function. Figures 4(a) and 4(b) display the probability density distribution corresponding to the conduction-band envelope function for an electron confined in a QD with structure displayed in Figs. 4(c) and 4(d). The probability density distributions of the $|HH\uparrow\rangle$, $|LH\uparrow\rangle$, and $|LH\downarrow\rangle$ components of the ground hole state $\psi_H^{\uparrow}$ [i.e., $|\langle u_n \,|\, \psi_H^{\uparrow}\rangle|^2 = |\chi_n(\boldsymbol{r})|^2$, see Eq. (1)] are shown in Figs. 4(e) and 4(f), Figs. 4(i) and 4(j), and Figs. 4(m) and 4(n), respectively. Note that the color scales are normalized to be able to observe features of the weak LH components. While the electron wave function and $|HH\uparrow\rangle$ envelope function strongly overlap, the donut-shaped $|LH\uparrow\rangle$ envelope function has only a weak overlap with them. Additionally, due to its in-plane quasiantisymmetry (not shown) its contribution to the optical matrix elements is close to zero. The same considerations apply to the $|LH\downarrow\rangle$ component.

In presence of strain with $\varepsilon = 0.1\%$ (Table II), the weight of the LHs is increased to 5.0% ($|LH\uparrow\rangle$) and 2.0% ($|LH\downarrow\rangle$). Strain modifies the probability density distributions of the $|HH\uparrow\rangle$, $|LH\uparrow\rangle$, and $|LH\downarrow\rangle$ components of the state $\psi_H^{\uparrow}$, which are displayed in Figs. 4(g) and 4(h), Figs. 4(k) and 4(l), and Figs. 4(o) and 4(p), respectively. (The electron wave function is only negligibly modified by the strain and is not shown.) While the $|LH\uparrow\rangle$, which is mostly induced by the quantum confinement (as discussed above), still has negligible overlap with the electron wave function [Figs. 4(k) and 4(l)], the strain-enhanced $|LH\downarrow\rangle$ [Figs 4(o) and 4(p)] has a sizable overlap with the electron and exhibits in-plane quasisymmetry. Therefore, it contributes to the optical transitions and leads to the DE brightening. The corresponding transition dipole is oriented along the growth direction, as observed experimentally. To avoid confusion, we also note that the exciton is still mostly heavy-hole-like with a small contribution of light holes and differs considerably from the purely light-hole exciton studied in Ref. [17].

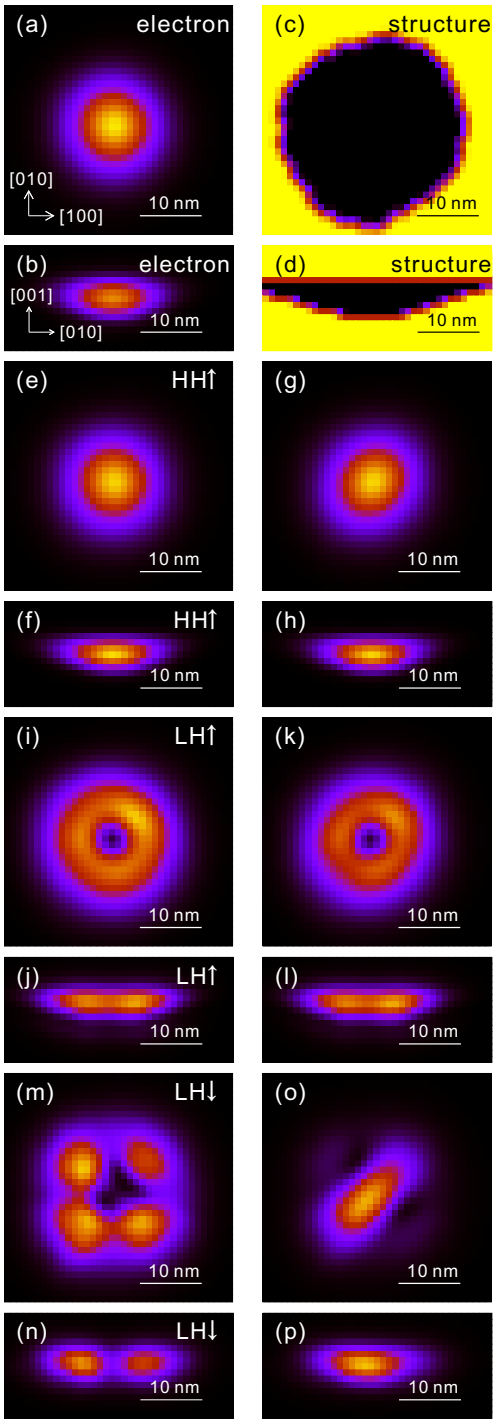

FIG. 4. Significant envelope functions (represented by probability density distributions) of the ground spin-up electron and hole states in a GaAs QD with a height of 6.6 nm. (a) and (b) electron, $|S\uparrow\rangle$ component. (c) and (d) QD planar cross sections on the (001) plane through the midheight and on the (1-10) plane through the center, respectively (black: GaAs, yellow: $Al_{0.4}Ga_{0.6}As$). (e)–(p) Components of the spin-up hole ground state $\psi_H^{\uparrow}$: $|HH\uparrow\rangle$ with no strain (e) and (f) and with an additional uniaxial strain ($\varepsilon = 0.1\,\%$) along the [1–10] direction (g) and (h); $|LH\uparrow\rangle$ with no strain (i) and (j) and with strain (k) and (l); $|LH\downarrow\rangle$ with no strain (m) and (n) and with strain (o) and (p). The two-dimensional graphs are constructed by integrating the density over the third (nondisplayed) coordinate. The color scale is normalized to the respective maxima.

It is instructive to discuss the envelope functions of different components of the ground hole state from the point view of symmetry. We introduce the total angular momentum $F = J + l^{\chi}$ of a particle as a sum of its zone-center Bloch wave total angular momentum J and the envelope function angular momentum l^{χ}. For a cylindric symmetry of the confinement potential (or as long as the deviation is small, which is the case of zero strain), the z projection of the total angular momentum F_z is a good quantum number and every component of the Luttinger spinor carries the same value of F_z. The dominant component of the valence-band spin-up ground-state $\psi_H^{\uparrow}$ is $|HH\uparrow\rangle$ with $J_z = +\frac{3}{2}$. The corresponding envelope function has $l_z^{\chi} = 0$, resulting in $F_z = +\frac{3}{2}$. Consequently, the envelope functions for $|LH\uparrow\rangle$ and $|LH\downarrow\rangle$ components (with $J_z = +\frac{1}{2}$ and $-\frac{1}{2}$) must have angular momentum l_z^{χ} of $+1$ and $+2$, respectively. The value of 1 for l_z^{χ} of the $|LH\uparrow\rangle$ is responsible for the node in the center of the density distribution (a donut shape of the envelope function) in Figs. 4(i) and 4(j). On the other hand, when external stress is applied, the symmetry is reduced and F_z is no longer a good quantum number. For that reason, the envelope function for the $|LH\downarrow\rangle$ component in Figs. 4(o) and 4(p) has $l_z^{\chi} = 0$ character. It has therefore nonzero spatial integral with the electron and renders the DE optically active.

The above discussion, which is based on noninteracting single electrons and mixed holes in our QDs, allows us to understand the origin of the observed brightening of DEs. However, the Coulomb, exchange, and correlation interactions must be taken into account to achieve a quantitative and complete description of the excitonic spectrum of QDs, i.e., the transition energies and decay rates. As an example, the above arguments are not sufficient to explain why only one of the two originally dark excitons is brightened (see Tables I and II).

VI. EFFECTS OF QD SIZE ON DARK EXCITON INTENSITY AND EMISSION ENERGY

The size of the QD affects the optical activity of the DE (in small QDs, the DEs remain dark, for larger QDs they become bright although no quantitative trend was experimentally observed) and the dark-to-bright exciton energy separation (which decreases with increasing QD size as shown in Fig. 2).

The fact that the strain brightens the DE more effectively in large QDs can be explained as follows. While the HHs and LHs are degenerate in the bulk, quantum confinement introduces an energy splitting between confined HH and LH levels. The larger the QD, the smaller is the splitting. For a particular value of anisotropic in-plane strain (and thus for the same magnitude of the mixing term in the Hamiltonian) the HH-LH mixing is more effective for small HH-LH splitting, i.e., in large QDs. This naturally results into a stronger optical activity of the DE. This conclusion is supported also by the simulations, as shown in Figs. 3(a) and 3(c).

Next, we discuss the dependence of ΔE_{DB} on the QD size. In Fig. 2 we show both experimental and theoretical values of ΔE_{DB} as functions of the exciton transition energy, which is used to represent the QD size (lower transition energy corresponds to taller QD and vice versa). We see that our calculations reproduce well both the magnitude of ΔE_{DB} and its increase with decreasing QD height. Note that strain has minor effects on ΔE_{DB}, as mentioned above. The increase of ΔE_{DB} with decreasing size (increasing emission energy) is attributed to the stronger Coulomb (and exchange) interaction in smaller QDs, which are characterized by more compact wave functions. The spread of the experimental data collected on small QDs may be due to the strong sensitivity to the specific shape of the nanoholes.

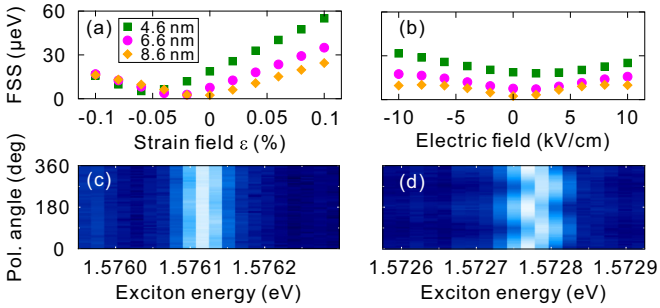

FIG. 5. (a) and (b) Calculated fine structure splitting (FSS) of the bright in-plane-polarized excitons as a function of strain (a) and electric field (b) for QDs with different sizes. (c) and (d) Representative color-coded polarization-resolved spectra (collected along the growth direction) of QDs, obtained by 2 nm GaAs filling, in the center and near the cleaved edge of a sample.

VII. EFFECTS OF CLEAVED FACET ON THE BRIGHT EXCITON FINE STRUCTURE SPLITTING

To further corroborate our conclusion that anisotropic strain is responsible for the brightening of DEs, we test here one prediction of our model, i.e., that the strain-induced symmetry reduction at cleaved facets leads to a sizable increase of the FSS of the bright doublets. Figures 5(a) and 5(b) show the calculated FSS as a function of strain field and electric field, respectively. The strain field results into an increase of FSS while the effect of an in-plane electric field is much smaller. Figures 5(c) and 5(d) show representative polarization-resolved spectra of QDs in the center and close to the edge (within 1 μm) of a 3 mm $\times$ 3 mm sample, respectively. In this case, μ-PL spectra were acquired with excitation and collection along the growth direction. Already from the raw data we see an increased FSS for QDs close to the sample edge, as expected. This observation is confirmed by measuring the FSS of several QDs [28]. The agreement between experiments and calculations supports our conclusions on the effects of strain and our explanation of the brightening of DE in the GaAs QDs.

VIII. CONCLUSION

In conclusion, we have reported on the observation of dark excitons confined in GaAs QDs close to a cleaved facet. The DEs are clearly visible in large dots and their energy separation from the dominant BEs tends to decrease with increasing QD size. We attribute the spontaneous brightening

of DEs to the symmetry breaking provided by anisotropic strain fields present at cleaved edges. Theoretical calculations using eight-band **k·p** theory reproduce well the experimental results and show that, while modest heavy-/light-hole mixing is already present in our QDs due to the quantum confinement, only anisotropic strain can lead to a significant brightening of the DEs. This work presents a straightforward method to access DEs in symmetric QDs, which may be used as long-lived states for spin storage in quantum technologies. At the same time it shows that both the hole mixing in QDs and the FSS of bright excitons are significantly affected by nearby edges. This means that even a cleaved edge suffices to make a dark exciton optically active, which has to be taken into account when a long lifetime of dark excitons is desirable or when integrating QDs in nanophotonic structures. On the other hand, we propose the possibility to have both optically active and inactive dark excitons on a single sample, where the patterning of the sample would allow their positions to be controlled. Finally, by relying on the progress in dynamic manipulation of strain in QDs [36,37], we envision the possibility of dynamically switching on/off a DE via application of anisotropic stress pulses.

ACKNOWLEDGMENTS

This work was financially supported by the FWF (project P29603), BMBF project QuaHL-Rep (Contracts No. 01BQ1032 and No. 01BQ1034), the European Union Seventh Framework Programme (FP7/2007-2013) under Grant Agreement No. 601126 (HANAS), and the Natural Science Foundation of Shanghai (Contract No. 17ZR1443900). Huo thanks the support of CAS 100 Talents Programme, V.K. was supported by the Ministry of Education of the Czech Republic, Project No. LQ1601 (CEITEC 2020). We thank E. Zallo and R. Engelhard for MBE assistance, A. Halilovic for SEM assistance, and J. X. Zhang, S. Kumar, and R. Trotta for discussions on the optical measurements.

[1] S. Lüker, T. Kuhn, and D. E. Reiter, Phys. Rev. B **92**, 201305(R) (2015).
[2] J. McFarlane, P. A. Dalgarno, B. D. Gerardot, R. H. Hadfield, R. J. Warburton, K. Karrai, A. Badolato, and P. M. Petroff, Appl. Phys. Lett. **94**, 093113 (2009).
[3] E. Poem, Y. Kodriano, C. Tradonsky, N. H. Lindner, B. D. Gerardot, P. M. Petroff, and D. Gershoni, Nat. Phys. **6**, 993 (2010).
[4] M. Goryca, P. Plochocka, T. Kazimierczuk, P. Wojnar, G. Karczewski, J. A. Gaj, M. Potemski, and P. Kossacki, Phys. Rev. B **82**, 165323 (2010).
[5] C. Gautham, D. W. Snoke, A. Rastelli, and O. G. Schmidt, Appl. Phys. Lett. **104**, 143114 (2014).
[6] M. Nirmal, D. J. Norris, M. G. Bawendi, A. L. Efros, and M. Rosen, Phys. Rev. Lett. **75**, 3728 (1995).
[7] M. Bayer, A. Kuther, A. Forchel, A. Gorbunov, V. B. Timofeev, F. Schäfer, J. P. Reithmaier, T. L. Reinecke, and S. N. Walck, Phys. Rev. Lett. **82**, 1748 (1999).
[8] M. Bayer, O. Stern, A. Kuther, and A. Forchel, Phys. Rev. B **61**, 7273 (2000).
[9] D. Gammon, Al. L. Efros, T. A. Kennedy, M. Rosen, D. S. Katzer, D. Park, S. W. Brown, V. L. Korenev, and I. A. Merkulov, Phys. Rev. Lett. **86**, 5176 (2001).
[10] M. Bayer, G. Ortner, O. Stern, A. Kuther, A. A. Gorbunov, A. Forchel, P. Hawrylak, S. Fafard, K. Hinzer, T. L. Reinecke, S. N. Walck, J. P. Reithmaier, F. Klopf, and F. Schäfer, Phys. Rev. B **65**, 195315 (2002).
[11] K. Kowalik, O. Krebs, A. Golnik, J. Suffczyński, P. Wojnar, J. Kossut, J. A. Gaj, and P. Voisin, Phys. Rev. B **75**, 195340 (2007).
[12] T. Smoleński, T. Kazimierczuk, M. Goryca, T. Jakubczyk, Ł. Kłopotowski, Ł. Cywiński, P. Wojnar, A. Golnik, and P. Kossacki, Phys. Rev. B **86**, 241305(R) (2012).
[13] M. Korkusinski and P. Hawrylak, Phys. Rev. B **87**, 115310 (2013).
[14] S. Kumar, E. Zallo, Y. H. Liao, P. Y. Lin, R. Trotta, P. Atkinson, J. D. Plumhof, F. Ding, B. D. Gerardot, S. J. Cheng, A. Rastelli, and O. G. Schmidt, Phys. Rev. B **89**, 115309 (2014).
[15] Y. H. Huo, A. Rastelli, and O. G. Schmidt, Appl. Phys. Lett. **102**, 152105 (2013).
[16] Y. H. Huo, V. Křápek, A. Rastelli, and O. G. Schmidt, Phys. Rev. B **90**, 041304(R) (2014).
[17] Y. H. Huo, B. J. Witek, S. Kumar, J. R. Cardenas, J. X. Zhang, N. Akopian, R. Singh, E. Zallo, R. Grifone, D. Kriegner, R. Trotta, F. Ding, J. Stangl, V. Zwiller, G. Bester, A. Rastelli, and O. G. Schmidt, Nat. Phys. **10**, 46 (2014).
[18] P. Lodahl, S. Mahmoodian, and S. Stobbe, Rev. Mod. Phys. **87**, 347 (2015).
[19] O. Stier, M. Grundmann, and D. Bimberg, Phys. Rev. B **59**, 5688 (1999).
[20] J. M. Luttinger and W. Kohn, Phys. Rev. **97**, 869 (1955).
[21] G. Bastard, Phys. Rev. B **24**, 5693 (1981).
[22] G. E. Pikus and G. L. Bir, Fiz. Tverd. Tela (Leningrad) **1**, 1642 (1959) [Sov. Phys. Solid State **1**, 1502 (1960)].
[23] O. Stier, Electronic and optical properties of quantum dots and wires, Ph.D. thesis, Technische Universitat Berlin, Berlin, 2001.
[24] T. Takagahara, Phys. Rev. B **62**, 16840 (2000).
[25] J. D. Plumhof, V. Křápek, L. Wang, A. Schliwa, D. Bimberg, A. Rastelli, and O. G. Schmidt, Phys. Rev. B **81**, 121309 (2010).
[26] V. Křápek, P. Klenovský, and T. Šikola, Phys. Rev. B **92**, 195430 (2015).
[27] L. Wang, V. Křápek, F. Ding, F. Horton, A. Schliwa, D. Bimberg, A. Rastelli, and O. G. Schmidt, Phys. Rev. B **80**, 085309 (2009).
[28] See Supplemental Material at http://link.aps.org/supplemental/10.1103/PhysRevB.95.165304 for details of the cleaved edge, intensity and polarization of the excitonic emissions, and excitonic fine structure splitting.
[29] G. P. Srivastava, Rep. Prog. Phys. **60**, 561 (1997).
[30] J. M. Dallesasse, N. Holonyak Jr., A. R. Sugg, T. A. Richard, and N. El-Zein, Appl. Phys. Lett. **57**, 2844 (1990).
[31] J. H. Luscombe and C. L. Frenzen, Solid-State Electron. **46**, 885 (2002).
[32] T. A. Germer, K. W. Kołasinski, J. C. Stephenson, and L. J. Richter, Phys. Rev. B **55**, 10694 (1997).
[33] As all our samples have no intentional doping, the depletion field from background doping is in fact rather small (∼3 kV/cm). Depletion length $W = [2\varepsilon\Phi/(e2N_d)]^{1/2}$, ε is dielectric

constant, Φ is surface potential energy barrier ($\sim$0.68 eV), e is charge of electron, and N_d is background doping density ($\sim 2.5 \times 10^{14}\,\mathrm{cm}^{-3}$).

[34] J. I. Climente, M. Korkusinski, G. Goldoni, and P. Hawrylak, Phys. Rev. B **78**, 115323 (2008).

[35] J.-W. Luo, G. Bester, and A. Zunger, Phys. Rev. B **92**, 165301 (2015).

[36] J. Martín-Sánchez, R. Trotta, G. Piredda, C. Schimpf, G. Trevisi, L. Seravalli, P. Frigeri, S. Stroj, T. Lettner, M. Reindl, J. S. Wildmann, J. Edlinger, and A. Rastelli, Adv. Opt. Mater. **4**, 682 (2016).

[37] F. J. R. Schülein, E. Zallo, P. Atkinson, O. G. Schmidt, R. Trotta, A. Rastelli, A. Wixforth, and H. J. Krenner, Nat. Nanotechnol. **10**, 512 (2015).